

Technical Report - Additional Experiment Results for Paper “Vehicle and Wheels Stability Defined Using Driving Envelope Protection Algorithm”

Denis Efremov, Martin Klaučo, and Tomáš Haniš ^{*}

1 Introduction

This document provides additional experiment results extending the “Experiments” section of the paper “Vehicle and Wheels Stability Defined Using Driving Envelope Protection Algorithm,” submitted to the IEEE TRANSACTIONS ON INTELLIGENT TRANSPORTATION SYSTEMS journal.

The mentioned paper aimed to utilize linear driving envelope [1] and model predictive control frameworks for vehicle stability. Provided simulation experiments show that the resulting control strategy could prevent wheel-locking, wheelspin, and wheel-skidding of all subjected wheels and overall of the vehicle. The experiments also show the robustness properties of the controller against a change in friction properties of the driving surface.

2 Experiment Setup

To simulate vehicle dynamics, we used IPG CarMaker software [2], which has compatibility with MATLAB/Simulink environment. The whole controller strategy from the paper is implemented in the Simulink environment. The optimal control problem is formulated in Matlab and is solved using the qpOASES [3] solver. We used “DemoCar” as the test vehicle, the most common vehicle in CarMaker. The whole project used for the paper with the implementation of the control strategy in the Matlab/Simulink environment is available on GitHub in the same folder as this report. The test vehicle is operated by the basic programmed driver available in CarMaker software. We assume global brake and accelerator action with constant transfer between the pedal application and generated brake or drive torque on each wheel.

Firstly, to test the hypothesis that the proposed control strategy could prevent dangerous vehicle dynamics situations and provide functionality similar to ABS, TCS, and ESC systems at the same time, we offered four test scenarios in comparison to an uncontrolled car. Each test result and discussion are presented in a particular subsection. All videos of the provided comparison are available on our YouTube channel [4].

Secondly, we provide the same tests with our previous controller version from [1], which is called the baseline. The controller formulation for the baseline regulator is presented in a particular section. Separately, we show the comparison of the proposed controller with the previously used baseline controller on the same prediction horizon (short). Then, we show that the prediction horizon length plays a small role even for the baseline controller. Therefore, it can be shortened for the sake of simplicity of the optimal control problem.

Used notation is presented in the Table 1.

^{*}D. Efremov and T. Haniš, are with the Department of Control Engineering, Faculty of Electrical Engineering, Czech Technical University in Prague, 120 00 Nové Město, Czech Republic (e-mail: {denis.efremov, martin.klauco, tomas.hanis}@fel.cvut.cz)

[†]M. Klaučo is with the Institute of Information Engineering, Automation, and Mathematics, Slovak University of Technology in Bratislava, Radlinského 9 82137 Bratislava, Slovakia (e-mail: martin.klauco@stuba.sk)

Variable	Symbol	Units
Vehicle velocity	v	m s^{-1}
Sideslip angle	β	rad
Yaw rate	r	rad s^{-1}
Brake pedal application	b	%
Throttle pedal application	t	%
Steering angle of front wheels	δ	rad
Angular velocity of wheel	ω	rad s^{-1}
Load force	F_z	N
Traction force of wheel	$F_{x/y}$	N
Sideslip angle of wheel	α	rad
Slip ratio of wheel	λ	—
Used subscriptions		Subindex
Lateral or longitudinal direction		y or x
Front or rear axle		f or r
Left or right side		l or r

Table 1: Used notation

3 Comparison with Uncontrolled Car

3.1 Sine with Dwell

We provided sine with dwell test to test electronic stability control (ESC) functionality and lateral vehicle stability. It induces oversteering motion of the vehicle. The experiment started once the car reached the predefined velocity (we used 80 km/h). The steering wheel did sine-like activation to the left and then to the right. At the maximum amplitude of the right position, it dwells for 0.5 s. Finally, the steering wheel returned to its original position (see reference signal in Fig. 1).

The baseline uncontrolled vehicle failed the test (Fig. 1) and went into a dangerous skid (the vehicle trajectories are depicted in Fig. 2). On the other hand, the controlled vehicle successfully passed the test, as MPC predictively simultaneously prevented boundary violations for sideslip angles of the front and rear wheels. The controller performed a fast front axle steering action in the direction of the skid. How fast the steering angle changes is defined in the definition of the slew constraint in MPC. At the same time, the controller applied the throttle pedal to produce a longitudinal force on the front wheels. The throttle and brake pedal activations are rough due to the small tracking weights for the front axle angular velocity and the prediction window size used for the MPC configuration. However, the prediction horizon is sufficient to prevent the dangerous vehicle's skid situation.

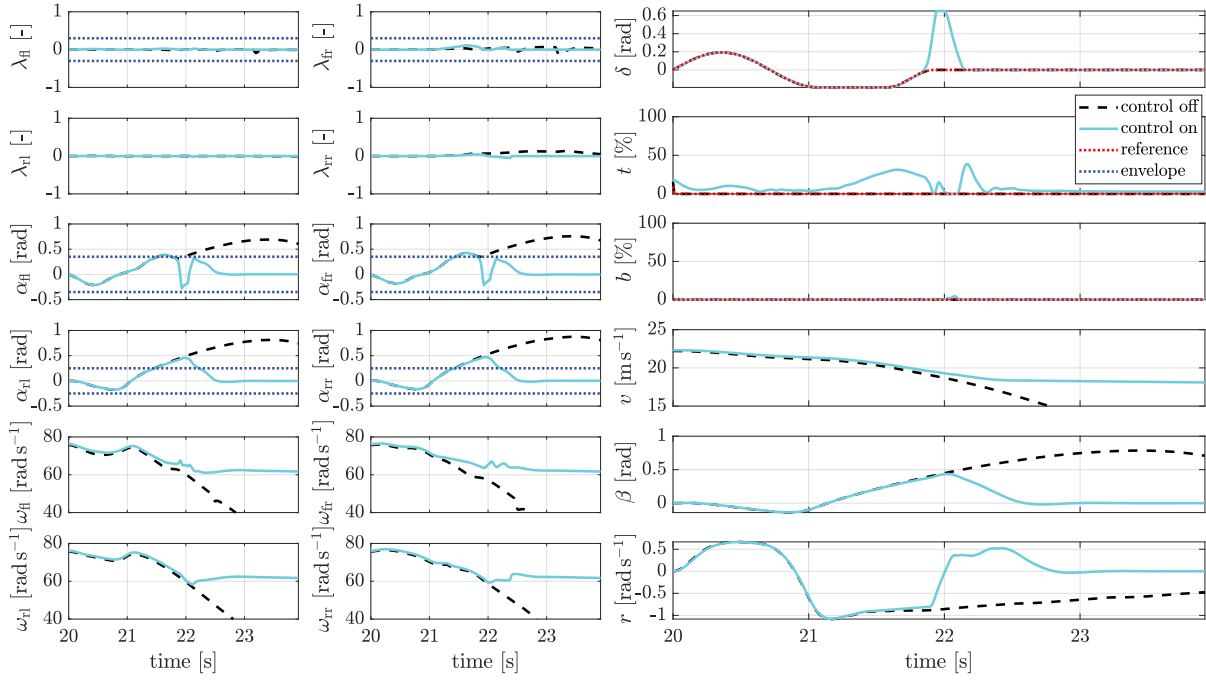


Figure 1: Sine with dwell at 80 km/h.

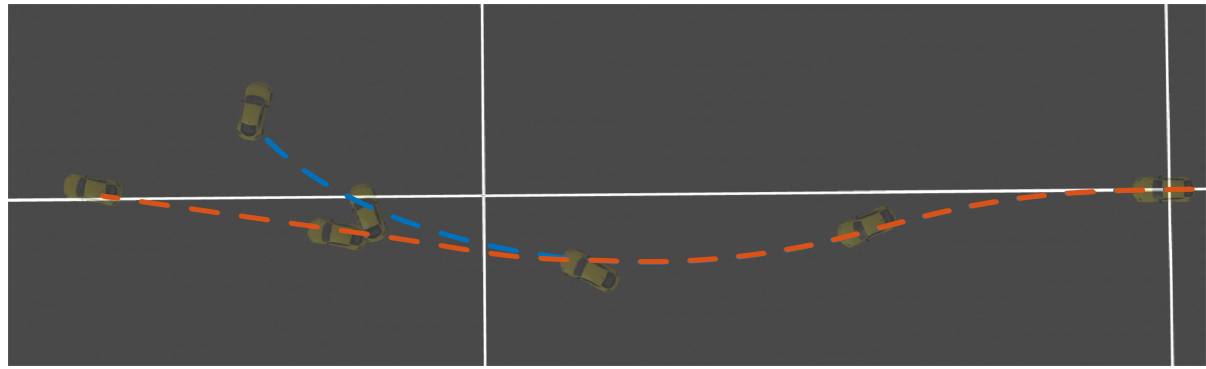


Figure 2: Vehicle trajectory during the sine with dwell test. Blue represents the trajectory of the uncontrolled vehicle, and orange represents the controlled vehicle.

3.2 Acceleration on a Slippery Surface with Sudden μ Change

In the second scenario, we provided a test of wheelspin protection, which is a typical traction control system (TCS) functionality. We performed an acceleration test on a slippery surface with a sudden change to asphalt (Fig. 3). The test data are presented in Fig. 5. The experiment started with the vehicle on a low friction surface ($\mu = 0.4$) at a standstill. The uncontrolled vehicle over-span the front axle due to the high engine torque. The uncontrolled car a bit outran the controlled one on the slippery surface. It is an effect of used tires: due to the shape of the slip curve presented in Fig. 4, the longitudinal traction force generated by the uncontrolled vehicle is a bit larger with a higher slip ratio on driven wheels. However, the controlled vehicle outran the uncontrolled when cars passed the slippery surface and came to the dry asphalt with nominal friction. It is the effect of unnecessary over-spin of driven wheels. Over-spun wheels must lose their angular velocity and “wait” until the car’s rigid body catches up with the wheel’s velocity. The controller provides better slip ratio allocation to generate more traction force by the front wheels, which causes faster acceleration on the asphalt segment. Notice that the friction coefficient estimation was not provided during the experiment. The controller uses the known parameter as the asphalt friction, which was equal to 1, instead of 0.4.

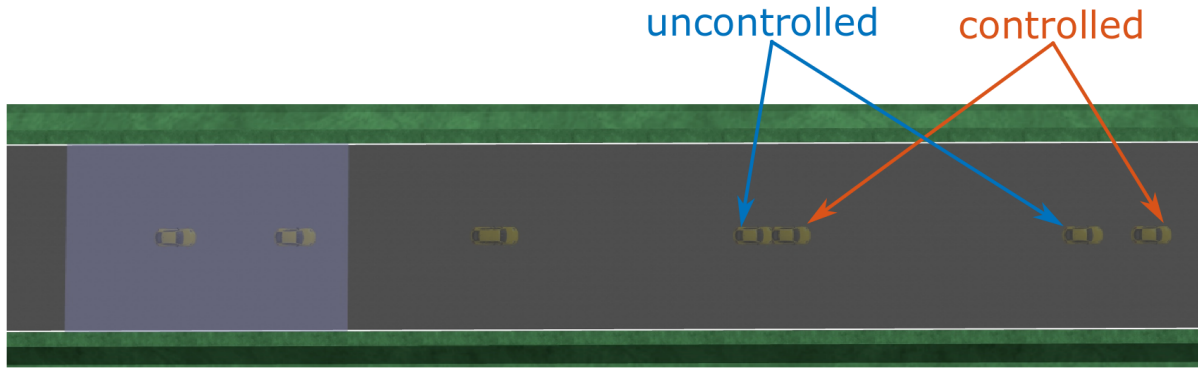


Figure 3: Vehicle trajectory during the acceleration test. Each pair of cars is presented after 2 seconds of motion.

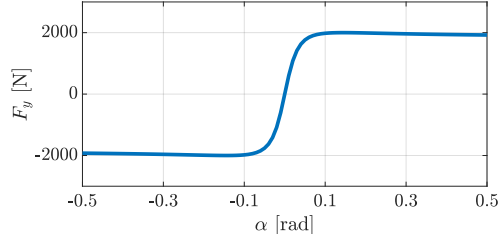


Figure 4: Longitudinal tire forces of test vehicle with load 2 kN.

Nevertheless, the general idea of wheelspin control is not about faster acceleration but about providing the driver with the possibility to control the vehicle laterally during fast acceleration. This also can be demonstrated in another experiment.

When the slip ratio of front wheels passes its peak value, the handling quality of front wheels in the lateral direction is significantly reduced because the lateral traction capabilities are exhausted. That could create dangerous situations once any lateral maneuver during acceleration is needed. Fig. 6 presents a car’s heading deviation after a step-like change of the steering wheel position during acceleration on a slippery surface. The controlled car had a better response on the steering wheel input during acceleration.

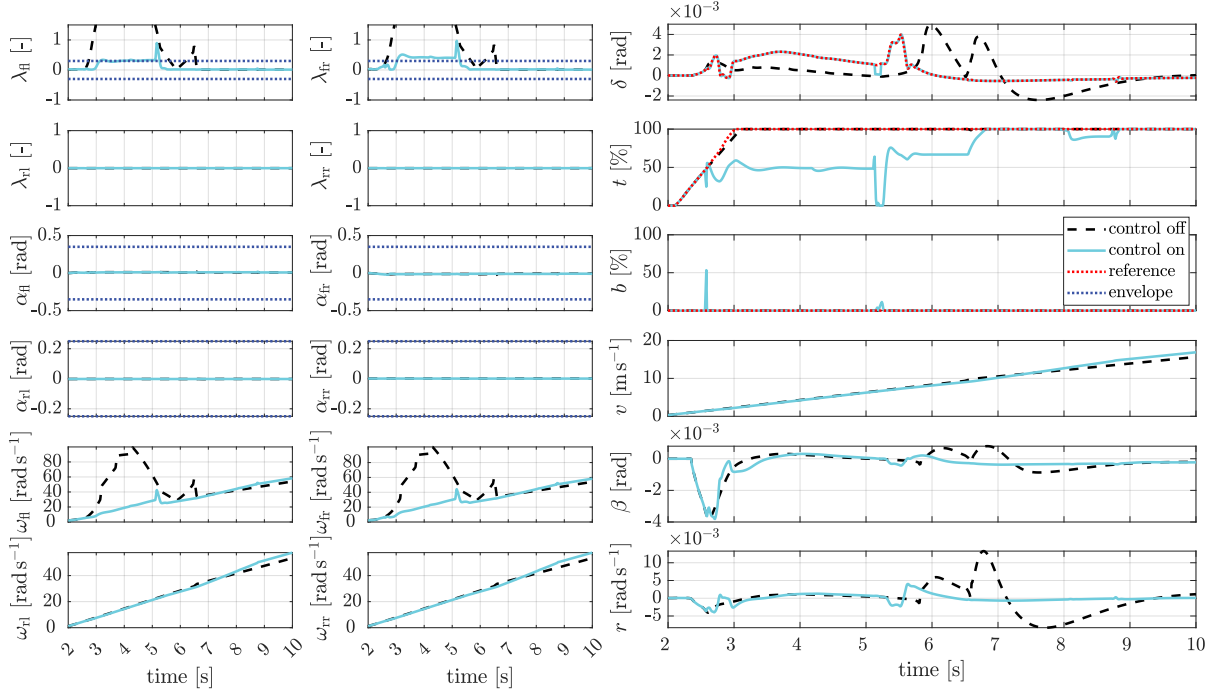


Figure 5: Acceleration on a slippery surface with $\mu = 0.4$ and sudden change to asphalt with $\mu = 1$ around 6.5 s.

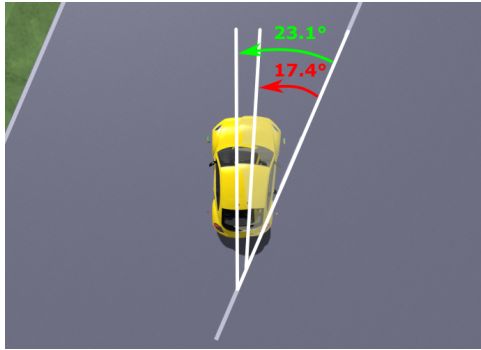


Figure 6: Lateral response of the vehicle with fully applied acceleration pedal. The ghost vehicle is uncontrolled. The proposed control structure controls the full-colored car.

3.3 Full Stop during Cornering Maneuver

A corner braking test (Fig. 7) analyzes the controller's ability to help in fast braking situations while cornering. When the vehicle turns during braking, one side generates more longitudinal traction force than the other due to the car's rotation. Because of this, there is a risk of the inner wheel becoming locked and uncontrollable (right in this case). Wheel-locking influenced the production of the lateral traction force. The driver could not stabilize the lateral vehicle dynamics using the steering wheel. All of these factors caused loss of vehicle maneuverability and sudden uncontrolled skidding behavior. The trajectory of the vehicle is depicted in Fig. 8.

On the other hand, the controlled vehicle did not lose traction because the front wheels stayed unlocked. It stopped without any loss of maneuverability. Notice that the used MPC did not protect the rear wheels. The right rear wheel was locked during the braking maneuver. Nevertheless, despite their vital value for lateral vehicle stability, the maneuver was stabilizable and controllable by the driver from the steering wheel.

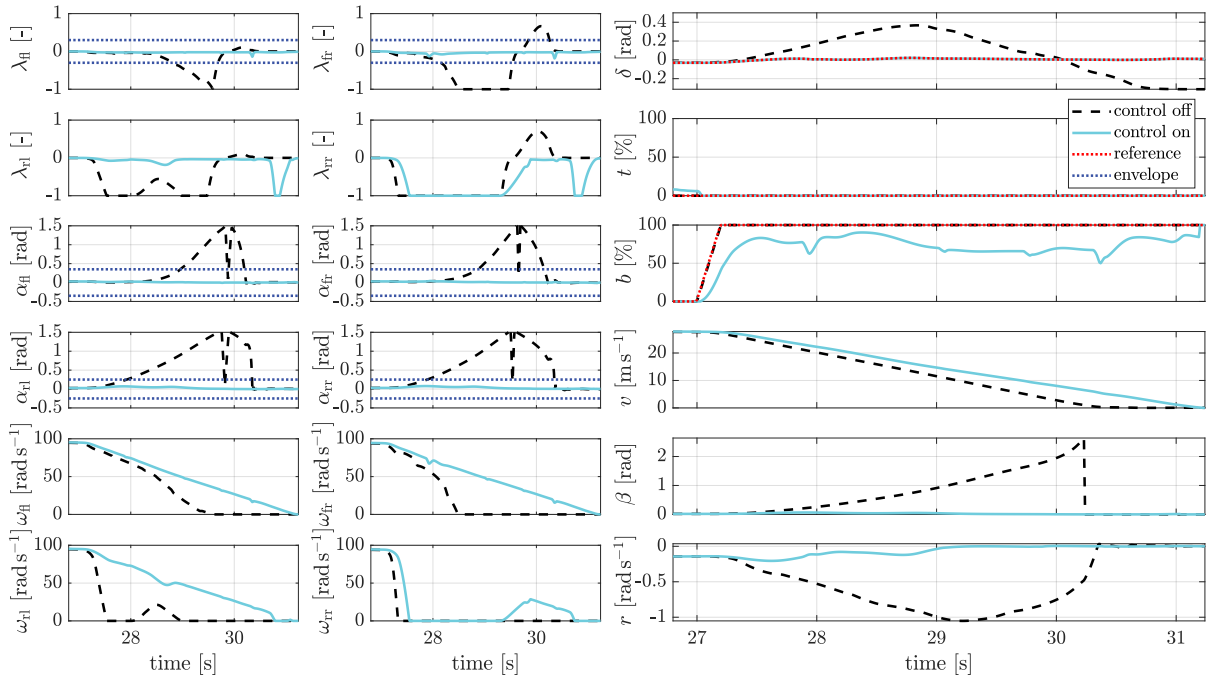


Figure 7: Braking on asphalt from 120 km/h during cornering maneuver.

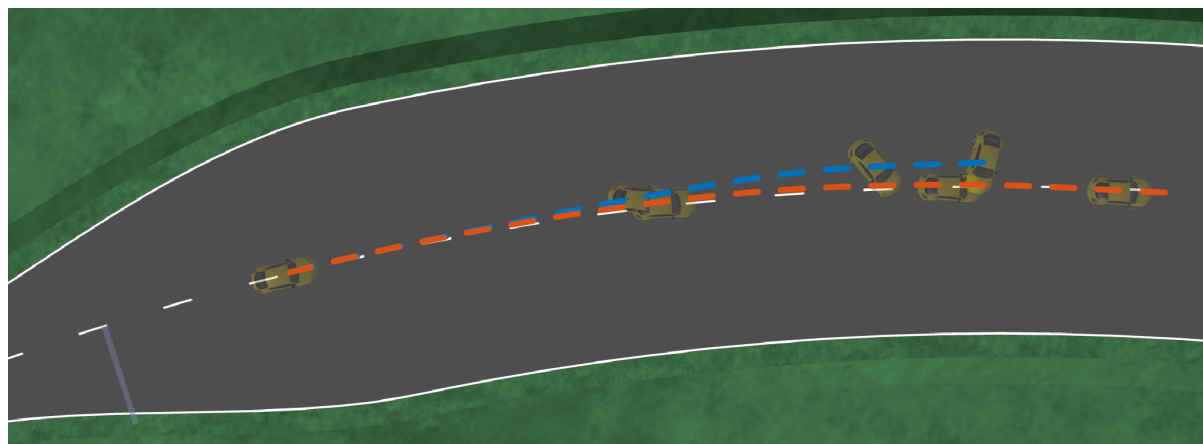


Figure 8: Vehicle trajectory during the braking test. Blue represents the trajectory of the uncontrolled vehicle, and orange represents the controlled vehicle.

3.4 Full Stop during Cornering Maneuver with μ -Split

To test the robustness of the used controller architecture against unknown friction, we enhanced the previously used corner braking test with a friction split pad (Fig. 9). The right side of the vehicle braked on a slippery surface with a friction coefficient equal to 0.4. The uncontrolled vehicle failed this test at the start of the braking maneuver due to locked right wheels. As a result, it suddenly went into an uncontrolled spin situation. Its trajectory is depicted in Fig. 10.

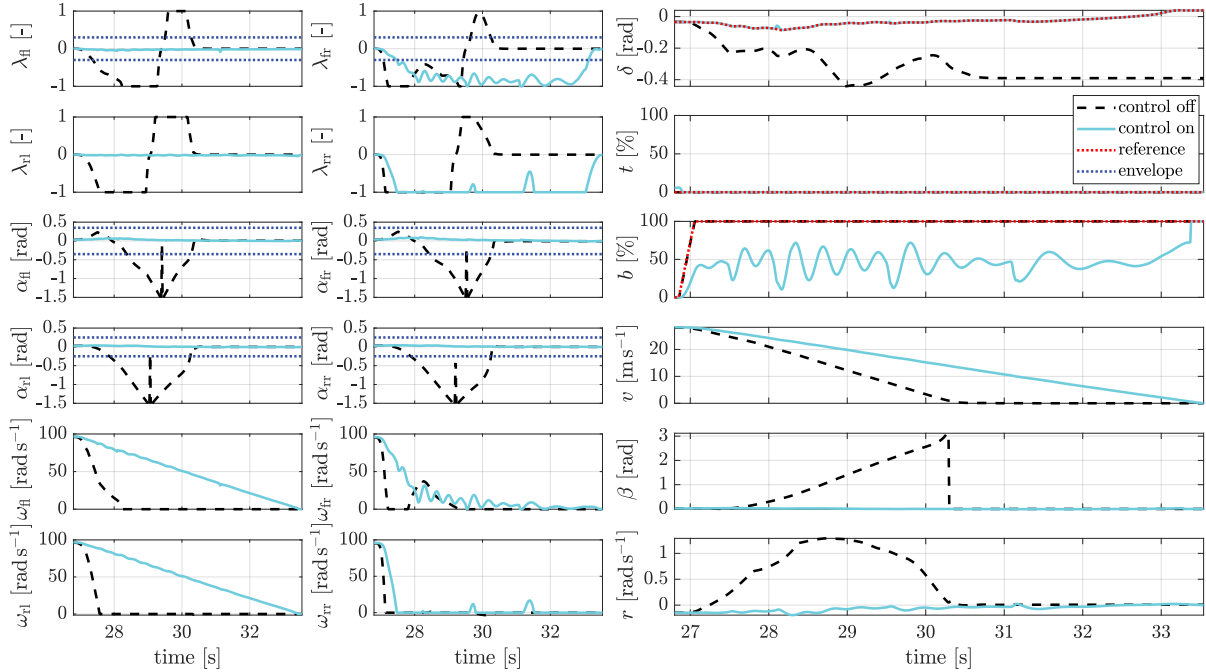


Figure 9: Braking on split surface from 120 km/h during cornering maneuver. The right side was on a slippery road with a friction coefficient equal to 0.4. The left side remained on asphalt with $\mu = 1$.

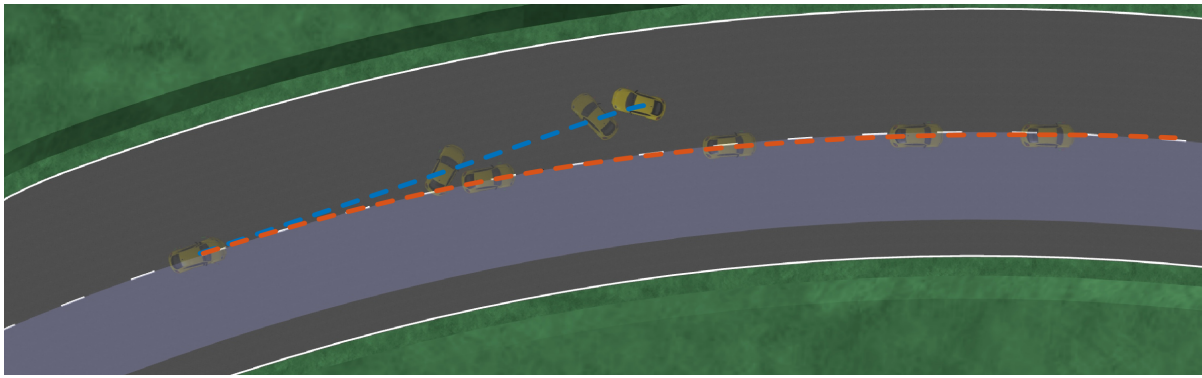


Figure 10: Vehicle trajectory during the braking with a split test. Blue represents the trajectory of the uncontrolled vehicle, and orange represents the controlled vehicle.

The controlled vehicle braked slower than in the previous test because it could not generate more traction force on the right side of the car. Nevertheless, the controller successfully prevented the front right wheel's locking without knowing the drivable surface's traction capability. Figure 11 presents normalized traction ellipses during this braking experiment. From this figure, we can admit that the

reason for slower braking is the lower traction capacities of the right side of the car. The controlled vehicle did not violate the traction ellipse boundaries. However, it caused less braking force generated on the slippery surface. The uncontrolled car acted on the wheel mounting point with force, which the tire cannot physically transfer to the place of contact with the surface. Thus, the traction ellipse boundary was violated, and the car suddenly went into an uncontrolled spin.

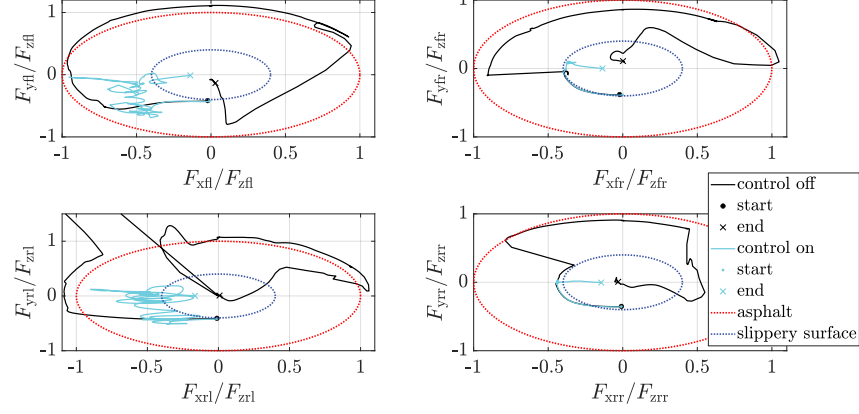


Figure 11: Normalized traction ellipses of wheels during split braking experiment.

4 Comparison with Baseline Controller

This report also presents a comparison of the new controller based on the outcomes presented in [5]. The previous version of the controller used separate constraints for the longitudinal and lateral slips of the subjected wheels. The new solution utilizes a combined slip definition that results in a fewer number of decision variables and occupies a smaller acceptable space within the vehicle state-space (see [5]).

The second difference is a shorter prediction horizon utilized in the new version of the controller, as it was shown that the control invariant set is reachable through a significantly smaller number of steps. This reduction in steps significantly decreases computational time, leaving the resulting controller with the ability to manage a safer level of stability.

However, to make both changes visible, we first present the change in the vehicle dynamics control due to changed constraints, and then, in the next section, we also discuss the value of the length of the prediction horizon.

4.1 Formulation of the Model Predictive Control for the Baseline Controller.

This subsection presents the MPC for the baseline (old version) of the controller, used in [1]. A detailed description of the variables used can be found in the submitted paper for which this technical report was written.

The MPC is formulated as a linear, convex, constrained finite-time optimal control problem:

$$\min_{u_0, \dots, u_{N-1}} \sum_{k=0}^{N-1} \left(R_1 |\rho - u_k| + (\rho - u_k)^T R_2 (\rho - u_k) \right. \\ \left. + (u_k - u_{k-1})^T R_{du} (u_k - u_{k-1}) \right) \quad (1a)$$

$$+ \sum_{k=0}^N [s_{i,k}^T Q_i s_{i,k} + s_{e,k}^T Q_e s_{e,k}] \quad (1b)$$

$$\text{s.t. } x_{k+1} = A_d x_k + B_d u_k, \quad (1c)$$

$$|u_k - u_{k-1}| \leq \Delta u_{\max} + s_{i,k}, \quad (1d)$$

$$|u_k| \leq u_{\max,k}, \quad (1e)$$

$$s_{i,k} \geq 0, \quad (1f)$$

$$|\lambda_{fl,k}| \leq \lambda_{fl,\max} + s_{ek}^{(1)}, \quad (1g)$$

$$|\lambda_{fr,k}| \leq \lambda_{fr,\max} + s_{ek}^{(2)}, \quad (1h)$$

$$|\alpha_{f,k}| \leq \alpha_{f,\max} + s_{ek}^{(3)}, \quad (1i)$$

$$|\alpha_{r,k}| \leq \alpha_{r,\max} + s_{ek}^{(4)}, \quad (1j)$$

$$s_{e,k} \geq 0, \quad (1k)$$

$$x_0 = x(t), \quad u_{-1} = u(t - T_s) \quad (1l)$$

The difference in the presented controller can be observed in (1f)-(1h). The rest of the control structure and used control parameters remain unchanged with respect to the submitted paper.

4.2 Sine with Dwell

The primary distinction between both control approaches is evident in how they handle steering actions (see Fig. 12). Due to its formulated approach regarding combined slip, the new controller permits minor breaches of the predefined lateral slip limits while still maintaining acceptable maneuver stability. In contrast, the baseline solution takes a proactive stance, preemptively reducing steering wheel input long before any potential breaches of lateral slip limits even become apparent. Consequently, this limits the overall lateral movement concerning yaw rate and sideslip angle.

Conversely, the latest iteration allows for swift actions in lateral dynamics but necessitates rapid steering movements in the opposite direction to stabilize the vehicle by the end of the experiment. Intriguingly, the prior solution began utilizing braking to stabilize vehicle movement, a tactic that could lead to undesirable driver experiences.

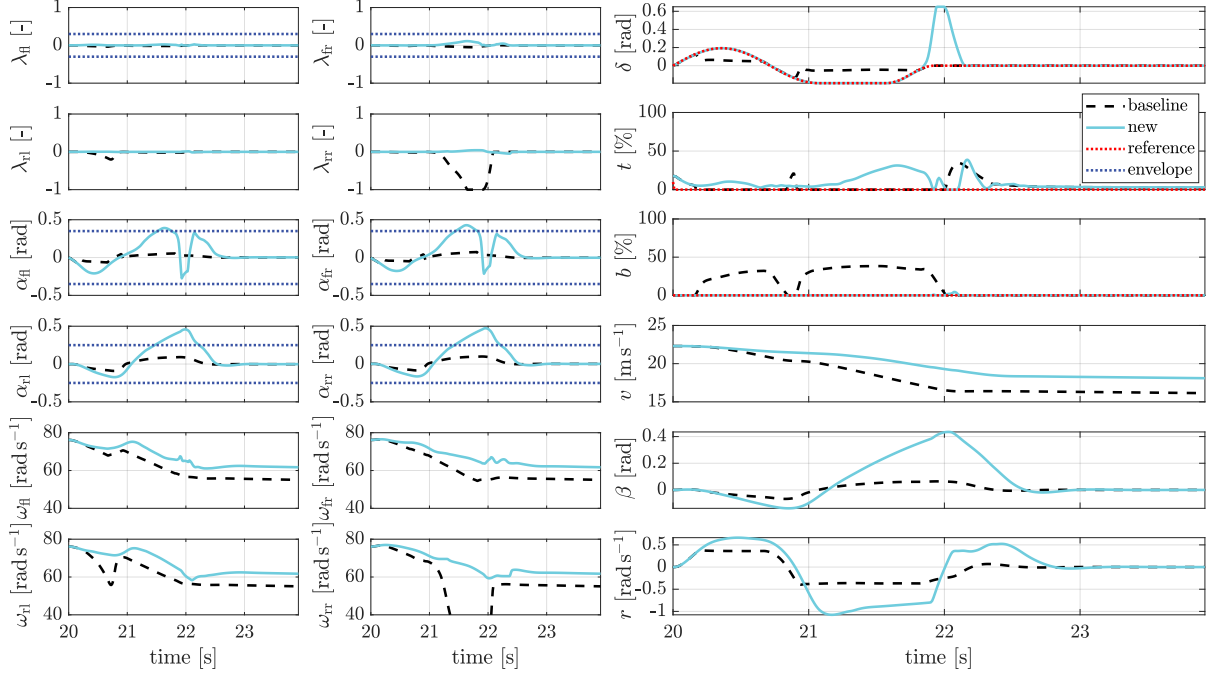


Figure 12: Sine with dwell at 80 km/h.

4.3 Acceleration on a Slippery Surface with Sudden μ Change

This experiment (Fig. 13) has only numerical differences between controllers as only one dynamics is involved here.

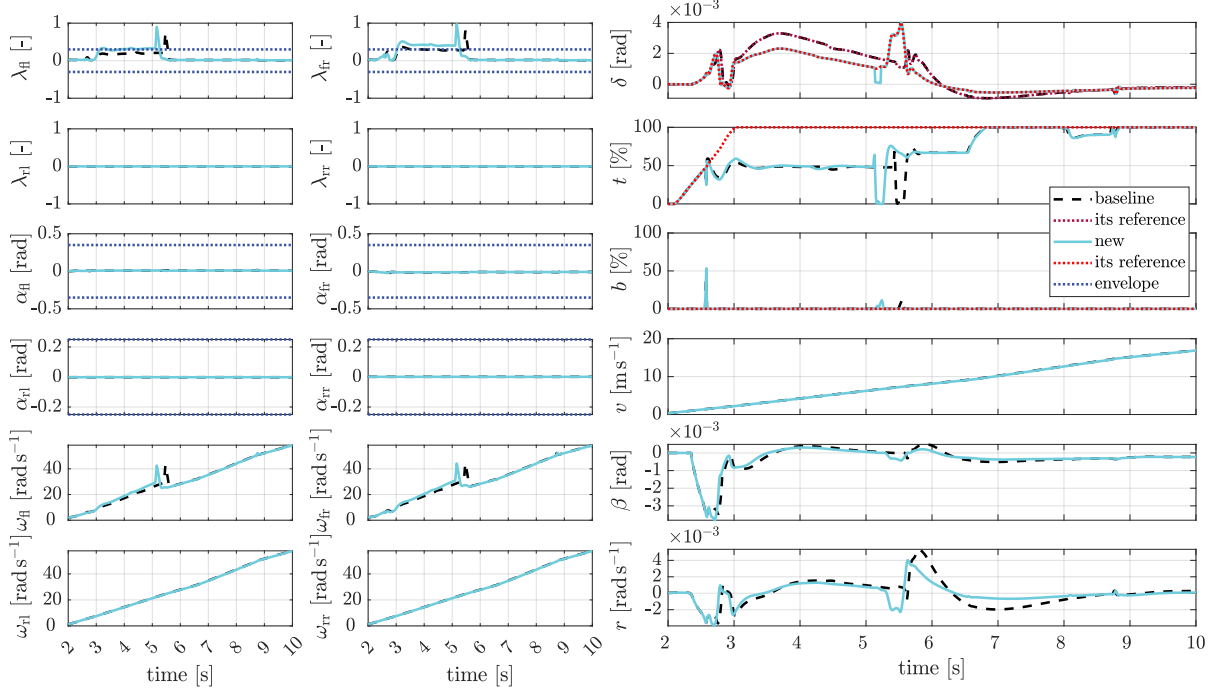


Figure 13: Acceleration on a slippery surface with $\mu = 0.4$ and sudden change to asphalt with $\mu = 1$ around 6.5 s.

4.4 Full Stop during Cornering Maneuver

This experiment (Fig. 14) also has no difference between controllers as both controllers did not approach the traction ellipse boundary during this maneuver.

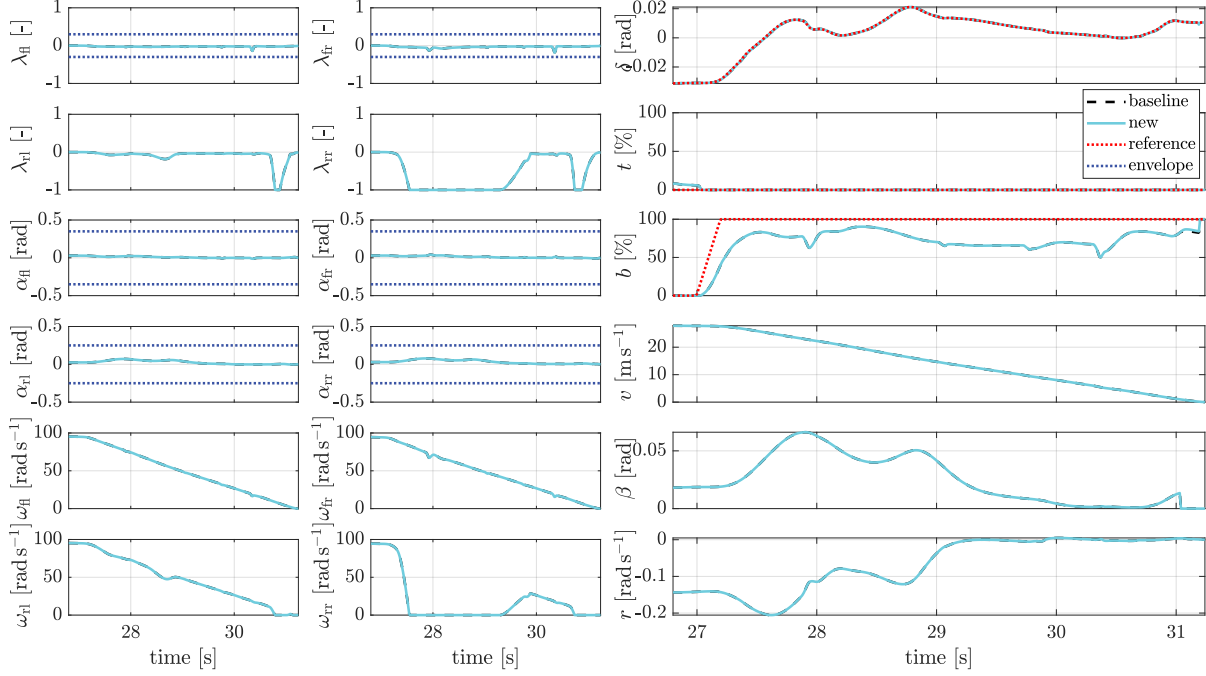


Figure 14: Braking on asphalt from 120 km/h during cornering maneuver.

4.5 Full Stop during Cornering Maneuver with μ -Split

In this experiment (Fig. 15), we can observe another distinction between the two controllers. Thanks to the new definition of the driving envelope [5], the new version carves out a smaller allowable space within the vehicle's dynamics state space. The key difference lies in combined slip, which mostly happens when the wheels are braking (or accelerating) and turning simultaneously, especially on a slippery surface.

The updated controller allows for slightly more breaches of the longitudinal driving envelope. However, it utilizes the left side of the vehicle more for the braking, as depicted in Fig. 16. The new definition of the combined slip constraints also results in small steering actions, which results in faster returns to the stable area. Consequently, there's a higher braking force on the left, enabling the vehicle to stop more swiftly. The braking distance was reduced by more than two car bodies (Fig. 17). Despite these differences, both scenarios ensure a stable maneuver.

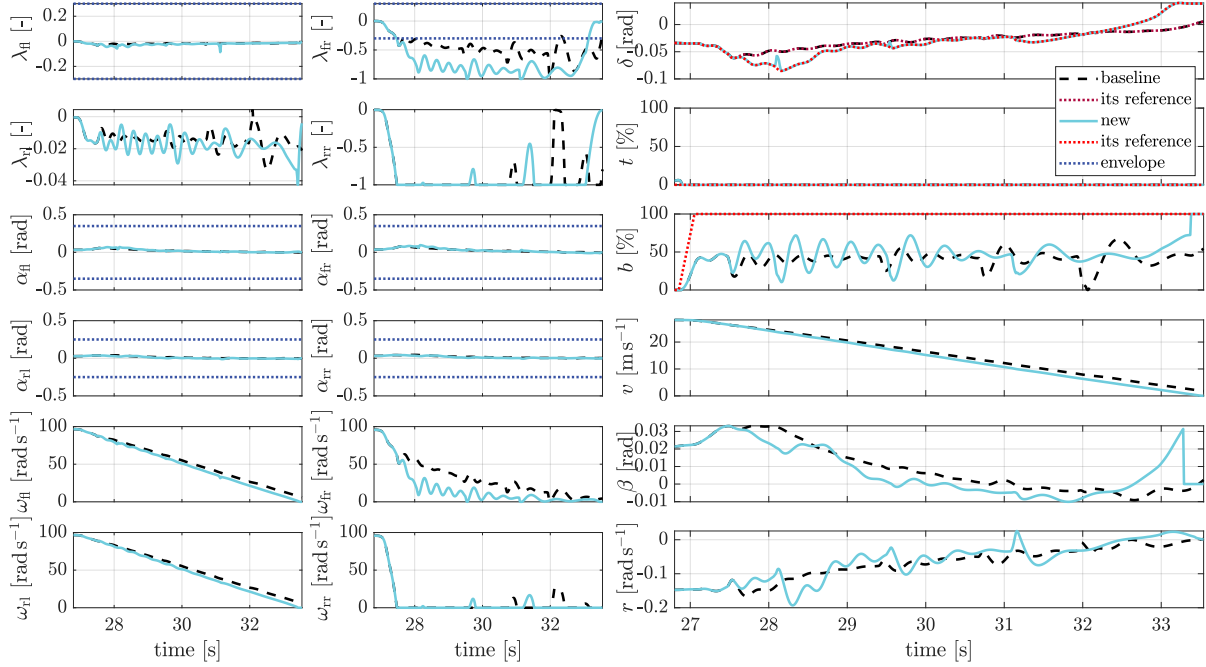


Figure 15: Braking on split surface from 120 km/h during cornering maneuver. The right side was on a slippery road with a friction coefficient equal to 0.4. The left side remained on asphalt with $\mu = 1$.

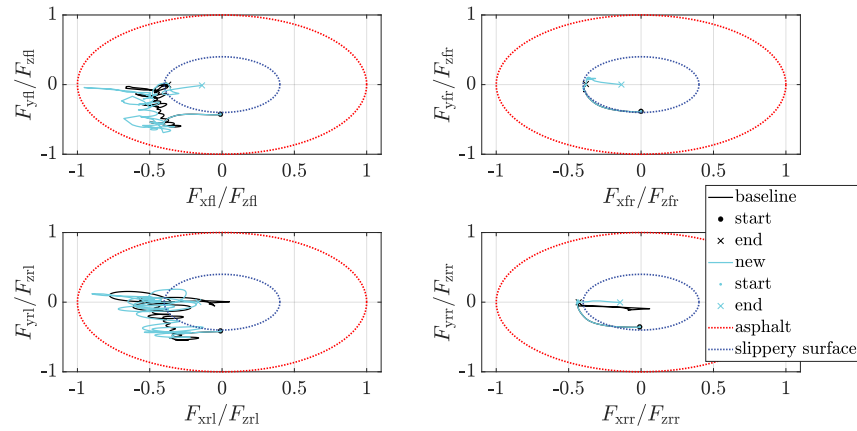


Figure 16: Normalized traction ellipses of wheels during split braking experiment.

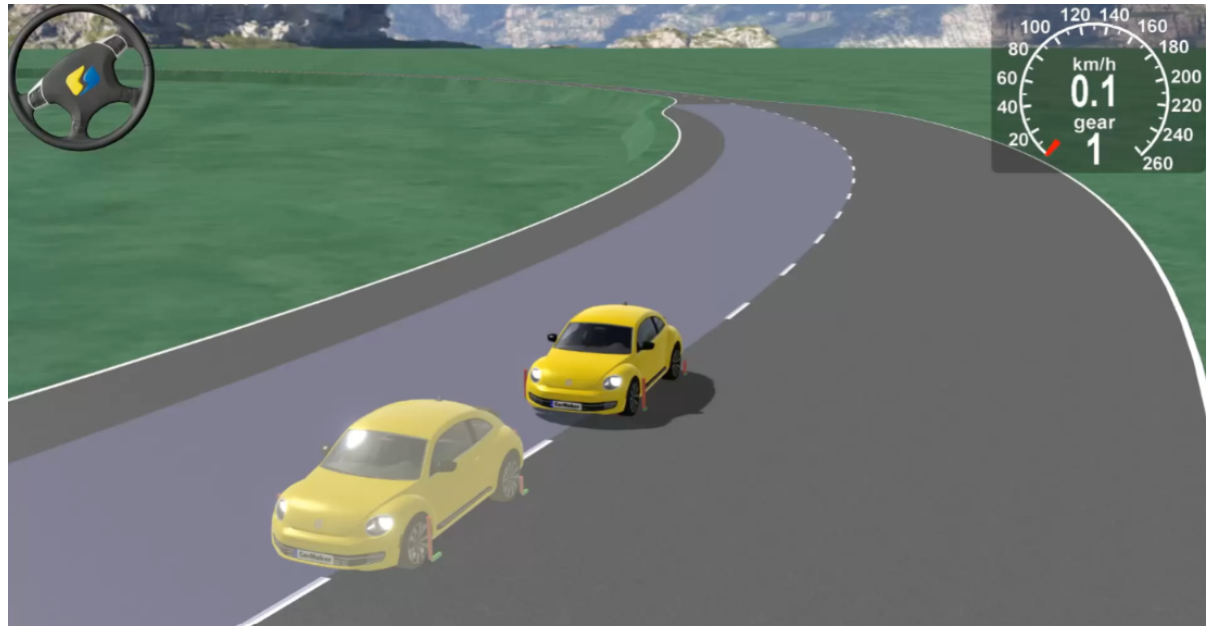


Figure 17: Conclusion of the braking experiments. The ghosted car depicts the baseline controller, while the fully colored vehicle illustrates the new controller.

5 Baseline Controller: on the Prediction Horizon

This chapter delineates the contrast between the baseline controller employed for short ($N = 3$) and long ($N = 10$) prediction horizons. Previously, as demonstrated in [5], we established the potential for a considerable reduction in prediction horizons for controllers of this type. In this chapter, we supplement these findings with experimental results to substantiate the theoretical outcomes.

To align with the alterations in the resultant objective function, we exclusively modified the weighting attributed to angular velocity tracking. The unaltered version of the controller necessitated a rebalancing between the tracking of two control variables: the angular velocity of the front axle and the steering wheel angle. Used weights are presented in Table 2. The rest remains unchanged.

Parameter	Symbol	Value for Long	Value for Short
Prediction horizon	N	10	3
Reference tracking linear weight	$R_1^{(2)}$	0.005	0.008
Reference tracking quadratic weight	$R_2^{(2)}$	0.005	0.008

Table 2: Changed control variables

5.1 Sine with Dwell

Typically, the primary disparity between these two controllers lies in the smoother control action offered by the 'longer' controller. This experiment, presented in Fig. 18, distinctly highlights this aspect compared to others. Specifically, in this scenario, the 'longer' controller demonstrates reduced utilization of the braking pedal. Nevertheless, the overall maneuver performance remains consistent across both controllers.

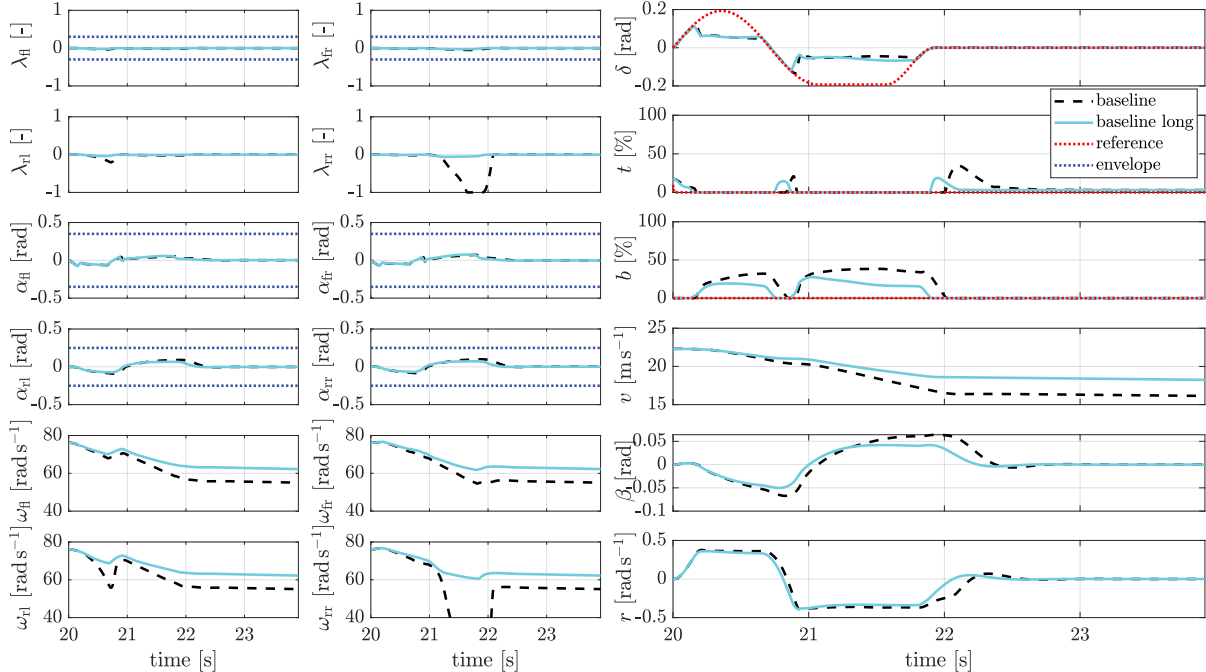


Figure 18: Sine with dwell at 80 km/h.

5.2 Acceleration on a Slippery Surface with Sudden μ Change

This experiment (Fig. 19) has only numerical differences between both controllers.

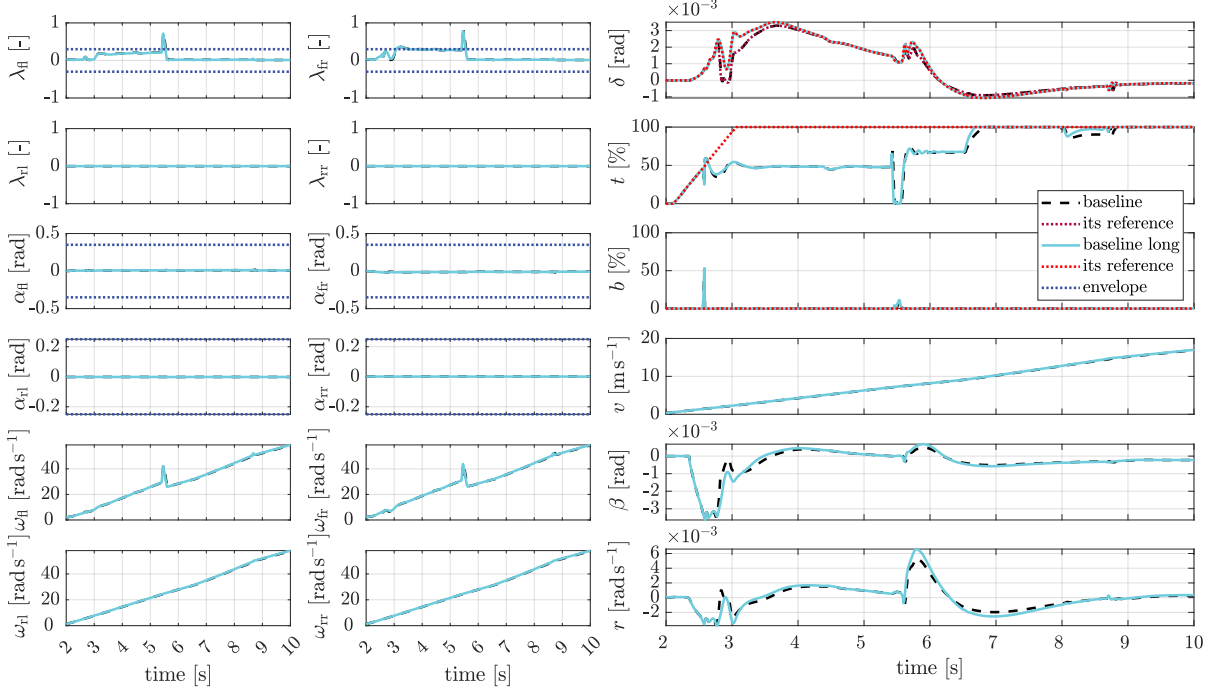


Figure 19: Acceleration on a slippery surface with $\mu = 0.4$ and sudden change to asphalt with $\mu = 1$ around 6.5 s.

5.3 Full Stop during Cornering Maneuver

Intriguingly, within this experiment (Fig. 20), the ‘longer’ version of the baseline controller displays a notably more aggressive tendency to apply braking compared to the ‘shorter’ version. Consequently, this prompts the driver to exert additional stabilization efforts through the steering wheel, which were successfully executed. Remarkably, despite these adjustments, the maneuver’s stability remained uncompromised.

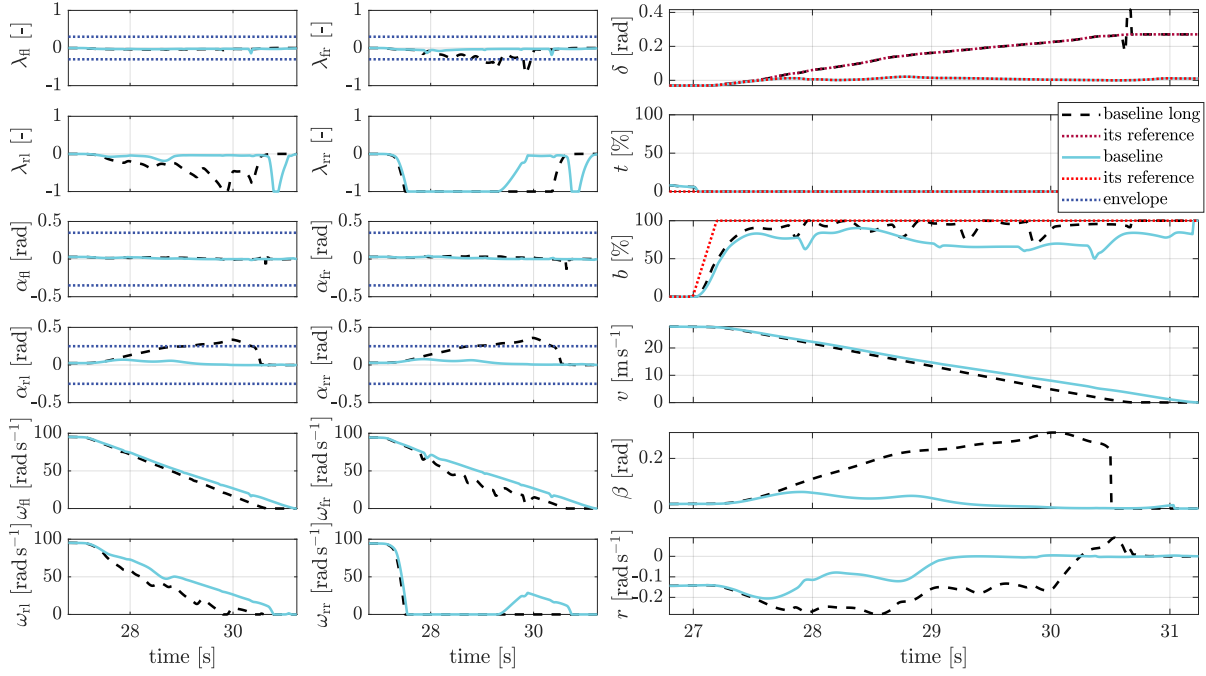


Figure 20: Braking on asphalt from 120 km/h during cornering maneuver.

5.4 Full Stop during Cornering Maneuver with μ -Split

This experiment (Fig. 21) has only numerical differences between both controllers.

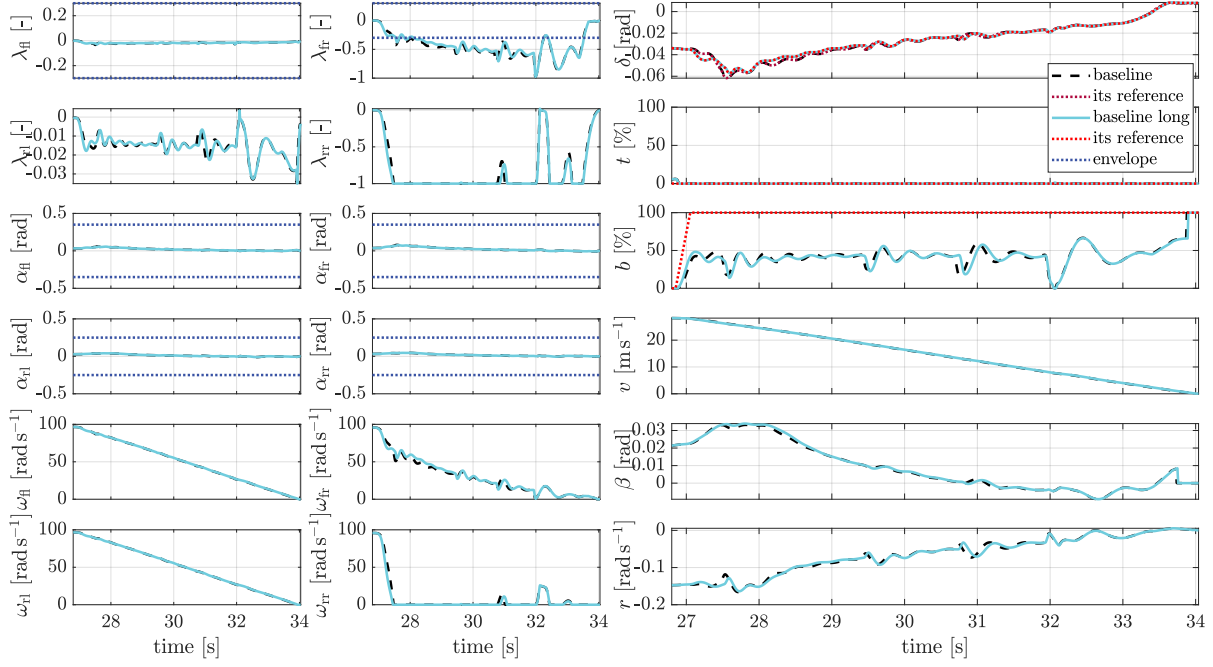


Figure 21: Braking on split surface from 120 km/h during cornering maneuver. The right side was on a slippery road with a friction coefficient equal to 0.4. The left side remained on asphalt with $\mu = 1$.

6 Acknowledgment

This work was supported in part by the Toyota Research on Automated Cars in Europe; in part by the Grant Agency of the Czech Technical University in Prague under Grant SGS22/166/OHK3/3T/13; in part by the Slovak Research and Development Agency under Project Danube strategy 2019 DS-FR-19-0031 and APVV-20-0261; in part by the Ministry of Education, Youth and Sports of the Czech Republic under Project 8X20037.

References

- [1] D. Efremov, M. Klaučo, T. Haniš, and M. Hromčík, “Driving envelope definition and envelope protection using model predictive control,” in *Proc. of the American Control Conference*, Denver, CO, USA, 2020.
- [2] IPG Automotive GmbH. (2023) Carmaker official website. [Online]. Available: <https://ipg-automotive.com/en/products-solutions/software/carmaker/>
- [3] H. J. Ferreau, C. Kirches, A. Potschka, H. G. Bock, and M. Diehl, “qpOASES: A parametric active-set algorithm for quadratic programming,” *Mathematical Programming Computation*, vol. 6, no. 4, pp. 327–363, 2014.
- [4] SDS, FEE, CTU in Prague. (2023) Smart driving solution’s youtube channel. [Online]. Available: <https://www.youtube.com/@smartdrivingsolutions3633>
- [5] D. Efremov, M. Klaučo, and T. Haniš, “Driving envelope: On vehicle stability through tire capacities,” in *2022 IEEE Intelligent Vehicles Symposium (IV)*. IEEE, 2022, pp. 1188–1193.